ORIGINAL PAPER

Poroelastic Properties of Sierra White Granite

Xuejun Zhou[1] · Ahmad Ghassemi[1]

Abstract

In this work, poroelastic properties of Sierra White granite namely elastic moduli, Biot's effective stress coefficient, α, and Skempton's pore pressure coefficient, B, are determined. The Biot's coefficient of this rock was determined using two different approaches. It is found that overall, the Biot's coefficient decreases from 0.77 at low effective stress (3–4 MPa) to 0.45–0.55 at high effective stress levels (30–40 MPa). Unlike the Biot's effective stress coefficient, which is related only to the solid rock, Skempton's B is a property related to both solid rock and the pore fluid. Although a single undrained hydrostatic compression test can theoretically be used to measure B, two types of laboratory tests were performed to fully reveal this parameter's behavior. In the first test, back pressure and confining pressure are increased stepwise to maintain a constant effective stress (usually very low), and Skempton's B is measured at different back pressure levels. This test reveals the Skempton's B behavior related to pore fluid compressibility, and consequently, this test can be used to evaluate if the pore fluid is free of air. In the second test, the back pressure is maintained at a constant level, and the confining pressure is increased stepwise, and then Skempton's B is determined at different confining pressure levels. This test correlates Skempton's B with effective stress. Details of the laboratory test protocol for combining these two types of tests are described and the results for Sierra White granite are provided. It is also found that the dead volume of the drainage system during the undrained compression test for the measurement of Skempton's B has an obvious impact on the measurement accuracy, with smaller dead volume yielding more accurate results.

Highlights

- The development of laboratory test protocol for Skempton's B measurement with consideration of both fluid and solid properties by two types of tests under two different boundary conditions.
- A comparison of using two different approaches to measure the Biot's effective stress coefficient.
- Determination of Biot's effective stress coefficient, α, and Skempton's pore pressure coefficient, B, for Sierra White granite.

List of symbols

α	Biot's effective stress coefficient
σ^{eff}	Effective stress
σ	Stress
ϕ	Porosity
ε_v	Volumetric strain
ζ	Pore fluid content
ρ_f	Pore fluid density
ρ_{fL}	Fluid density in the drainage system
C_d	Elastic compressibility coefficient of rock, $c_d = 1/K$
C_s	Elastic compressibility coefficient of rock, $c_s = 1/K'_s$
C_L	Isothermal compressibility of the drainage system, $c_L = \frac{1}{V_L}\left(\frac{\partial V_L}{\partial P_f}\right)_{T,\sigma}$
K_L	IIsothermal compressibility of the drainage system, $\kappa_L = -\frac{1}{V_L}\left(\frac{\partial V_L}{\partial \sigma}\right)_{T,p_f}$
B	Skempton's B

✉ Ahmad Ghassemi
    ahmad.ghassemi@ou.edu

[1] Reservoir Geomechanics, Seismicity Group, The University of Oklahoma, Norman, OK, USA

H	Poroelastic expansion coefficient
H_L	Reciprocal of the isothermal compressibility of the drainage system, $H_L = 1/c_L$
K	Drained bulk modulus
K_L	Reciprocal of the isothermal compressibility of the drainage system, $K_L = 1/\kappa_L$
K_f	Pore fluid bulk modulus
K_s'	Grain bulk modulus
$1/K_s''$	Unjacketed pore compressibility
P_c	Confining pressure
P_P	Pore pressure
P_f	Fluid pressure (including pressure in the drainage system)
V	Rock volume
V_ϕ	Pore volume
V_L	Drainage system dead volume

1 Introduction

Two key parameters that are of interest for the poroelastic analysis in rock are Skempton's B and Biot's effective stress coefficient, α (Biot 1941; 1957; Skempton 1954; Ghassemi et al. 2009; Cheng 2016). If a fluid-saturated porous rock undergoes undrained hydrostatic compression, the confining pressure causes the pores to contract, thereby pressurizing the trapped pore fluid. The magnitude of this induced pore-pressure increment is described by the following equation (Berge et al. 1993; Skempton 1954; Cheng 2016):

$$B = \frac{\Delta P_p}{\Delta P_c}\bigg|_{\Delta\zeta=0} \tag{1}$$

where ζ is the pore fluid content (zero implies undrained conditions), P_c and P_p are confining pressure and pore pressure, respectively. It should be noted that Skempton's B is related with both rock matrix and pore fluid properties. In fact, the shapes of the porous spaces in the rock matrix can be diverse (sphere, needle, disk, cracks, etc.), and for crystalline rocks, the porosities are mostly attributed to open intra- and intergranular micro-cracks (Brace et al. 1972; Mavko et al. 2009).

The relationships among Skempton's B and compressibility or drained bulk moduli of bulk rock, solid grain, and pore fluid, as well as porosity, have been investigated by many researchers (Brown and Korringa 1975; Rice and Cleary 1976; Bishop 1973; Berryman and Milton 1991; Berge et al. 1993). And the relationship among these quantities can be described as:

$$B = \frac{\frac{1}{K} - \frac{1}{K_s'}}{\frac{1}{K} - \frac{1}{K_s'} + \phi\left(\frac{1}{K} - \frac{1}{K_s''}\right)} \tag{2}$$

where ϕ is the porosity, K is the drained bulk modulus of rock, K_s' is the solid grain bulk modulus or unjacketed solid frame bulk modulus, $1/K_s''$ is the unjacketed pore compressibility, which is defined as $K_s'' = -V_\phi(\partial P_f/\partial V_\phi)_{dP_f=dP_c}$; and K_f is pore fluid bulk modulus. If all grains in the rock are composed of the same material, $K_s' = K_s''$ (Berge et al. 1993). It is believed that any difference between K_s' and K_s'' is a result of deviation from an ideal porous material assumption, which refers to such a type of material with a uniform, isotropic and linearly elastic solid phase and a fully connected porous space (Cheng 2016; Makhnenko et al. 2017; Tarokh et al. 2018). Note in this equation, both fluid property (K_f) and rock frame property (K,K_s',K_s'') can all have impact to B. When the fluid compressibility is extremely small (such as gas with $K_f \to 0$), the denominator could become very large thus making B very small. That is, a variation of pore fluid could result in a fluctuation of Skempton's B.

The Skempton's B that is commonly referred to in the literature is usually based on the condition of water as the pore fluid. The Skempton's B coefficient allows the coupling between mechanical deformation and pore pressure to be quantified (Jaeger et al. 2007). Several experimental studies suggested that B usually decreases with effective stress and can cover a range from 0.9 to as low as 0.3 or so for some sandstones (Berge et al. 1993; Blöcher et al. 2007; 2014; Hart and Wang. 1995; 2001; 2010).

Biot's effective stress coefficient, α, is a key parameter that quantifies the contribution of the pore pressure to the effective stress. Biot's coefficient is a property of the solid and the porous frame only, which is independent of the fluid properties (Cheng 2016; Coussy 2004). Thus, the types of pore fluids (water, gas, or a mixture of different fluids) have no impact to the Biot's coefficient's measurement provided no physical/chemical reactions take place between the rock frame and the pore fluid(s). Assuming the effective-stress law is known, then the rock behavior can be measured at one pore pressure (often zero) and subsequently predicted for any other pore pressure. The Biot's effective stress law is usually given as (Biot 1941; Biot and Willis 1957):

$$\sigma^{eff} = \sigma - \alpha P_p \tag{3}$$

where σ is the stress, and σ^{eff} is the effective stress. Biot's effective stress coefficient has been measured for many different types of rocks using various methods based on different formulas (Blöcher et al. 2014; Cheng et al. 1993; 1997; Zhou et al 2015; 2017 and Zhou and Ghassemi 2022). A widely used formula for the estimation of the α is the following equation:

$$\alpha = 1 - \frac{K}{K_s'} \tag{4}$$

Since both K and K'_s are rock solid properties, α is independent of the pore fluid from a theoretical standpoint.

In another approach, α is expressed as a ratio of the drained bulk modulus K and the poroelastic expansion coefficient H (Biot and Willis 1957; Wang 2000).

$$\alpha = \frac{K}{H} \tag{5}$$

where H is called the poroelastic expansion coefficient, which describes how much the bulk volume changes due to a pore pressure change while holding the applied stress constant (note that Wang (2000) names H as the reciprocal of poroelastic expansion coefficient, and here we refer H as poroelastic expansion coefficient for simplicity. We also treat H as an absolute positive number). Poroelastic expansion coefficient is the ratio of pore pressure change over the volumetric strain under a constant confining pressure condition.

$$H = \frac{\Delta P_p}{\frac{\Delta V}{V}} = \frac{\Delta P_p}{\Delta \varepsilon_V}\bigg|_{\Delta Pc=0} \tag{6}$$

This parameter can be measured in the laboratory by conducting a pore fluid depletion test. Furthermore, a hydrostatic compression test for measuring K and a hydrostatic depletion test for measuring H can form a pair of tests for the measurement of α provided the confining and pore pressure levels are comparable for these two types of tests.

In this paper, we measured the Skempton's B and Biot's coefficient α for the low porosity low permeability rock Sierra White Granite, as few measurements of poroelastic parameters of tight crystalline rock are available in the literature (Mesri et al.1976; Hart and Wang 2001). This paper presents methods for sample preparation and saturation, determining four independent poroelastic parameters: the drained bulk modulus, the grain bulk modulus, poroelastic expansion coefficient, and Skempton's B coefficient under two different boundary conditions (maintain constant effective pressure/increase back pressure; maintain constant back pressure/increase effective pressure), which allow the fluid and solid properties' impacts to this parameter to be separated and revealed.

2 Sample Information

Sierra White Granite is mined and quarried from the granite rich Sierra Nevada mountain range in the USA, and is widely used as a construction material and in rock

Table 1 Sample information

| Sample No	Length (mm)	Diameter (mm)	Weight (g)	Density (g/cm^3)
A	73.40	37.70	215.51	2.63
C	68.60	37.70	202.02	2.63

mechanical studies. The samples information is summarized in Table 1 and Fig. 1. The samples porosities are about 0.80% with extremely low permeability, in the nano-Darcy range (Hu and Ghassemi 2020; Ye and Ghassemi 2018). These samples appear to be isotropic. The mineralogy information by XRD is listed in Table 2.

3 Laboratory Test Procedure

Laboratory test procedures of Skempton's B and the Biot's effective stress coefficient are different and are described in the following two sections.

3.1 Skempton's B Measurement

Laboratory measurement of Skempton's B requires a full saturation of the rock samples. Based on the conventional saturation method and some previous studies (ASTM 2004; Hart and Wang 1995; Mesri et al. 1976; Tarokh et al. 2018),
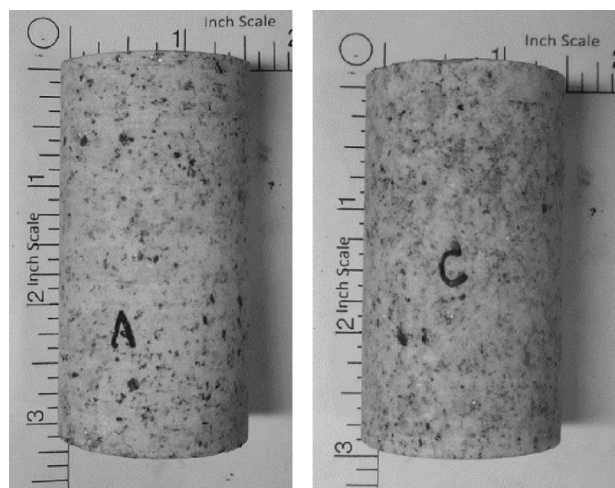
Fig.1 Sample image. These two samples are retrieved from a same block; Sample A was tested for Skempton's B and Sample C was tested for the Biot's effective stress coefficient. These two tests are independent with respect to each other. The Skempton's B measurement requires full water saturation on Sample A, while argon was used as the pore fluid for the Biot's coefficient measurement on Sample C

Table 2 Mineralogy of the Sierra White granite by XRD (Ye and Ghassemi 2018)

Sierra White granite	
Quartz	43.5%
Albite	46.1%
Sanidine	4.8%
Biotite	2.7%
Illite	2.0%
Clinochlore	0.9%

as well as our own experiences, we developed a saturation method with a focus on to minimize the air concentration in the pore water by different approaches at different stages.

For a rock of low permeability, the test of Skempton's *B* is difficult and challenging. Unlike Biot's coefficient, which is a property of the solid rock only, Skempton's *B* is influenced by both rock matrix property and pore fluid property. Using different pore fluids (water, oil, or water with different gas/air concentration) will yield different *B* values. To make the results reliable and more meaningful with respect to the real-world applications, pure water saturation is desired, although this could be quite difficult for rock samples of low permeability and porosity. The workflow we used is described by the following flowchart (Fig. 2).

The sample is prepared in a cylindrical shape with both end surfaces polished according to the rock mechanic test requirement. The standard tolerance is based on the International Tolerance (IT) grades table reference as ISO 286-1:2010 (2010). The recommended standard tolerance grade IT07 is followed as suggested by Feng et al. (2019); for a sample length in the range of 50 mm to 100 mm, the tolerance zone is 12.5 μm to 17.5 μm.

3.1.1 Initial Water Saturation Procedure Before Sample Jacketing

The test procedure is described in Fig. 3. The main parts of the experimental set-up include a vacuum pump (PITTS-BURGH, 3 CFM two stage vacuum pump), a syringe pump (Teledyne ISCO, 100DX), a steel chamber that can hold high fluid pressure (up to eight thousand psi), a water container, and a water cup. They are connected with the use of stainless-steel pipes and valves (V1–V6 in Fig. 3).

The following steps apply both negative pressure by vacuum and high pressure by syringe pump to remove the air in the sample during water saturation.

1) Prepare distilled and de-aired water for use in the pore system including the rock sample, the syringe pump, the water container and the associated pipes. The distilled water is supplied by the Rock Mechanics laboratory system of the university, and the water is further de-aired by a vacuum pump as low as a pressure of -25 psi.
2) Put the dry rock sample in a steel chamber, close the lid and seal the lid with grease. The lid is specially designed with two holes allowing fluid communication with the external devices. Vacuum this chamber using a vacuum pump by opening Valve 5 while closing all the other valves. Ensure that the water in the water container has also been de-aired. (Can also open Valve 1 to vacuum the water container at the same time if needed).
3) After two hours, close V1 (if it was opened), close V5, open V2 and then V4. The distilled/de-aired water in
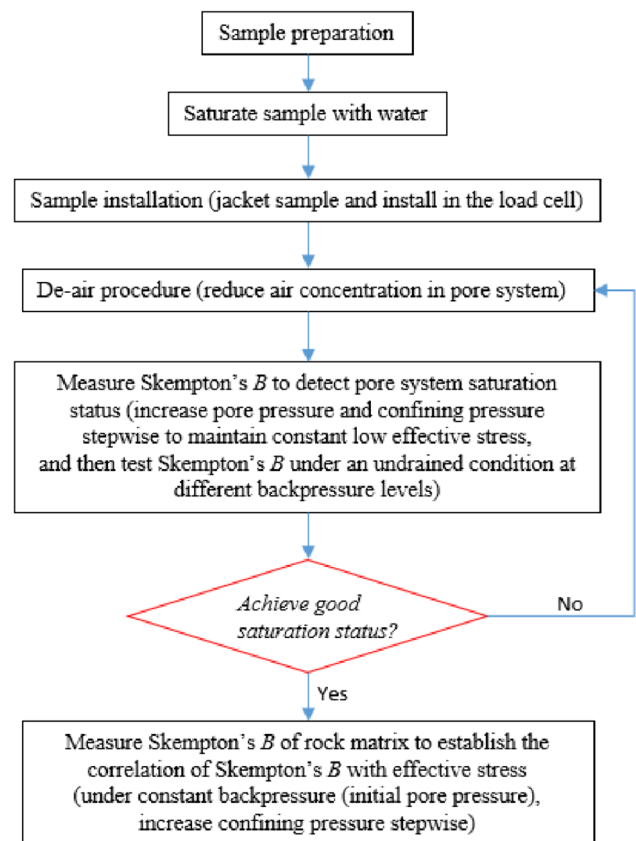
Fig.2 Laboratory test procedure flowchart (There are two sections of measuring the Skempton's B: the first one (the box above the red diamond box of decision) on the impact of pore fluid compressibility to the Skempton's B, and the second one (the box below the red diamond box) on the impact of rock structure to the Skempton's B)

the water container will be sucked by the negative air pressure (-20 psi in this case) inside the steel chamber to submerge the sample.
4) After the chamber is almost full of water with the rock sample totally submerged under water, lock the lid with clamps and bolts. The lid can be opened before locking to double check the water level to ensure the sample is fully covered by water.
5) After the lid is locked, close V4, open V5, run the vacuum pump to create a negative pressure in the chamber (generally -20 psi) and then close V5 to remain a vacuumed condition for the sample.
6) After 1 day or so, open V4 and V5, run the vacuum pump to further suck the water from the water container to the steel chamber until water appears in the pipe above the valve V5. Note that this section's pipe is transparent (made of stiff polyethylene) to allow the observation of water overflow. Another option is to use steel pipe but add a water trap in this section between the pump and V5 to avoid water overflow into the vacuum pump.
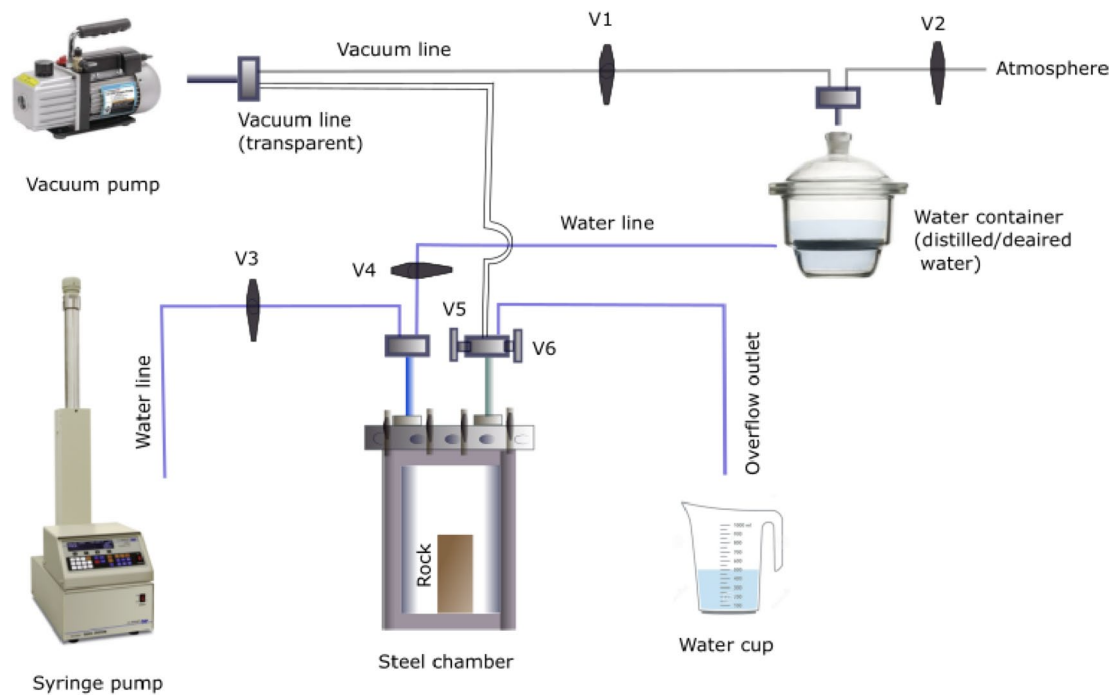
Fig.3 Schematic configuration of the water saturation set-up before sample jacketing

7) Once water overflow is detected, close V5 and V4, open V3 and V6, pump distilled/de-aired water from the syringe pump into the chamber and allow at least 80–100 ml water overflow to the water cup. And then close V6.

8) Further pump water into the steel chamber using the syringe pump to increase the fluid pressure up to 1000 psi and maintain the pressure for one day at least (the time can be much longer if the schedule is not tight). This pressure is believed to be high enough to be able to dissolve the air into water (Battino et al 1984) and enhance the saturation for a rock of low permeability.

9) During this time period, a fluid cycling process can be performed. Gradually reduce the fluid pressure to a very low level, open V6, and pump fresh de-aired water from the syringe pump to replace the old fluid in the steel chamber. Since both the inlet and outlet pipes are all connected to the lid, the fluid on the top region in the chamber will be replaced. If there is any trapped air in the chamber's fluid, this cycling is helpful to reduce the air concentration in the fluid. After a significant amount of fluid (at least 100 to 200 ml) overflowed to the water cup, the overflow line can be closed. Then, gradually increase the fluid pressure in the chamber to a high level (1000 psi) as before.

10) When the sample is ready for jacketing, gradually reduce the fluid pressure to the atmosphere condition and take the sample out of the chamber. Seal the sample with

two platens on both end surfaces and a very thin copper shim (0.076 mm) on the lateral surface with epoxy to cover the whole set-up for sealing. Note that the platens' empty space (holes in the platens) should also be filled with water before the sealing work. After the epoxy consolidates, put the sample into the MTS 810 cell, and move on to the next step.

3.1.2 De-airing Procedure After Sample Jacketing/ Installation

This step is illustrated in Fig. 4. This step aims to remove the air or at least reduce the air concentration as much as possible in the pore fluid system. The main parts include a MTS 810 core holder, a vacuum pump (PITTSBURGH, 3 CFM two stage vacuum pump), four Teledyne syringe pumps, a water container, an Agilent data acquisition system, a computer, and two pressure transducers (SMD P571 pressure sensor). They are connected and controlled with the use of pipes and valves (V1–V5 in Fig. 4). All the pore fluid-related parts (drainage lines, pressure transducers, platens, syringe pumps) must be flushed and filled with distilled/de-aired water before sample installation in the MTS 810 core holder.

11) Connect the bottom platen with one syringe pump filled with distilled/de-aired water (the upstream pump). Connect the top platen with a two-way valve (V4 and V5)
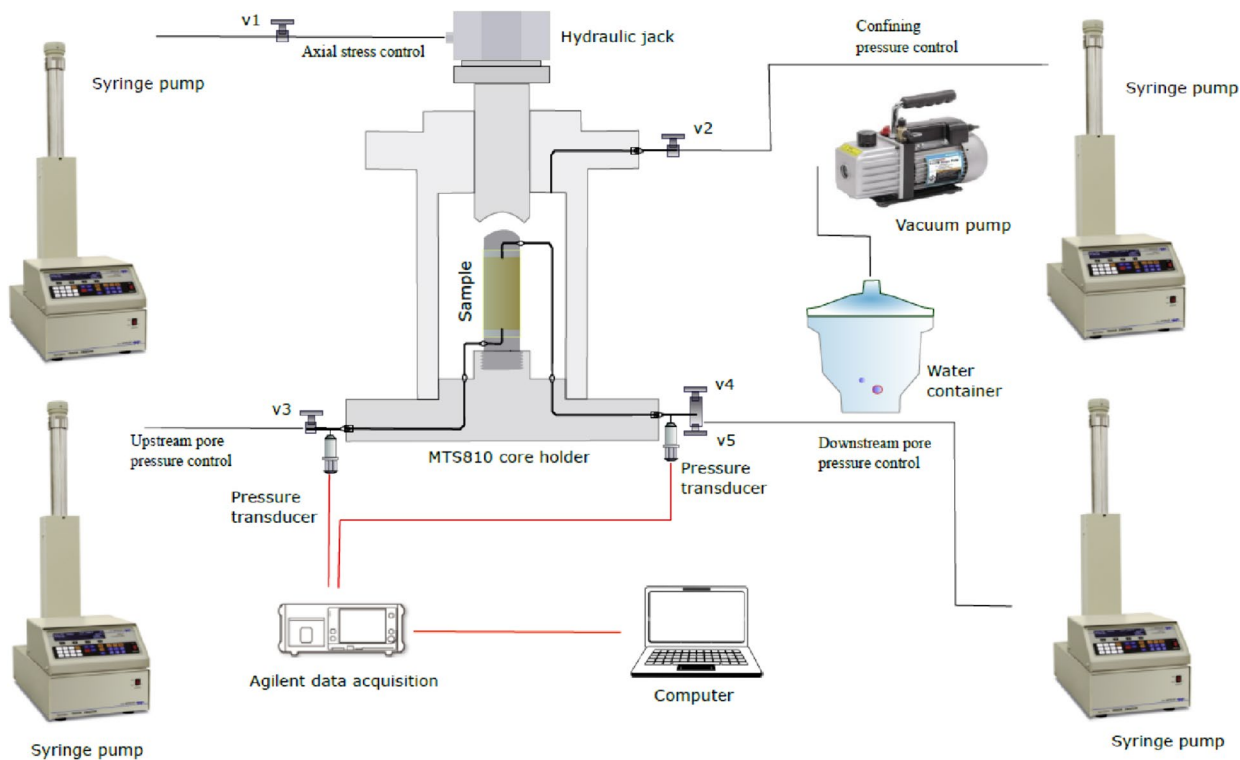
Fig.4 Schematic test configuration for Skempton's B measurement

which is further connected with a water container and a syringe pump, respectively; and connect this water container with a vacuum pump.

12) Close V1 and V5, open V2 to apply 500 psi confining pressure in the cell, and also apply 400 psi fluid pressure in the upstream pump with V3 opened. Open V4, create a negative pressure (-20 psi) in the water container by running the vacuum pump continuously.

13) Assuming the trapped air always tends to migrate upwards and is sucked by the vacuum pump, the fluid flow is expected to take the residual air out of the system. In fact, air foams can be observed in the chamber initially. The cover of the container is transparent to allow a direct observation of the inside of the container.

14) When no more air bubbles can be observed in the container, close V4, open V5. Increase confining pressure, upstream pump and downstream pump pressure to 1050 psi, 1000psi and 950psi, respectively. A low effective stress will allow a relatively high permeability in the sample. A high pore pressure is expected to further dissolve any trapped air in the rock. Allow a significant amount of water to flow through the sample. Depending on the rock permeability, fluid of 1–5 times of PV can pass through the sample within a reasonable time period (2–3 days or even longer). However, for an extremely low permeable rock such as Sierra White granite in this study, the core flooding process would be much longer. Thus using vacuum pump to suck the trapped air should be more frequent.

15) After a significant amount of pressurized flow has passed through the sample or at least 2–3 days' water flooding (in this case, one more week), reduce the pore pressure and confining pressure to 400 psi and 500psi, respectively. Close V5, open V4, run the vacuum pump and check if there are any more air bubbles in the water container. If some trace of air is still found, repeat the previous step. Otherwise, move on to the next step.

3.1.3 Skempton's *B* Measurement Under Different Backpressure but Similar Effective Stress

Although efforts have been made to achieve a very high saturation of the sample with very low air concentration in the pore fluid; a full (100%) saturation of the sample without any trapped air may not be reached. There is a threshold pore pressure beyond which the Skempton's *B* will be independent to the fluid pressure, indicating a linear pore-pressure measuring system. For a liquid (water), linear compressibility means the absence of free air (Mesri et al. 1976). The lower the threshold of the pore pressure to achieve such linearity, the higher the saturation degree of the sample with the pore fluid. Different techniques can be used to detect if

some air is still trapped to cause nonlinearity of the system. For example, if the pore pressure increases with the increase of confining pressure under an undrained condition initially but starts to decline (obviously) afterwards, this phenomenon indicates some air is still trapped in the system (Adachi 1974). On the other hand, if the system is depleted from air, then the Skempton's *B* would remain at a consistently high value insensitive to the change of back pressure under a constant effective pressure, as in this study and Mesri et al (1976). Determination of the threshold of pore pressure for linear fluid compressibility based on Skempton's *B* measurement is described below.

16) Ensure the valves V1 and V4 are closed, V2, V3 and V5 are opened. Set the upstream and downstream syringe pump pressures to the same value at 20 psi. Set the confining pressure at 100 psi, and the pore pressure can be taken as 20 psi under such a setting. Since the rock permeability is low, the pore pressure equilibrium inside the rock may take some time. Usually, a pore pressure equilibrium is indicated by a no flow condition between the rock sample and the pore pressure control pumps (both upstream and downstream pumps).

17) Close the valves V3 and V5 very slowly to avoid a pressure surge inside the sample and dead volume. If the pore pressure as detected by the two pressure transducers (right outside of the cell with the red lines connecting with an Agilent data acquisition machine (Fig. 4)) remain the same at 20 psi level (or less than 5% difference), a pressure equilibrium condition can be assumed to be reached under an undrained condition.

18) When the pore pressure equilibrium has been reached under an undrained condition (with valves V3 and V5 closed), increase the confining pressure from 100 to 150 psi, and record the change of pore pressure by the pressure transducers. The ratio between the pore pressure increment and the confining pressure increment (50 psi in this case) is taken as the Skempton's *B* at this step corresponding to a back pressure at 20 psi.

19) Increase the pore pressure to 120 psi while also increase the confining pressure to 200 psi at the same time to ensure the confining pressure constantly higher than the pore pressure. After pore pressure equilibrium has been reached at this stage, further increase the confining pressure to 250 psi with the sample under an undrained condition. Record the corresponded pore pressure increase and get the Skempton's *B* at this step. Repeat the step (17) and (18) in a stepwise manner until successive values of the Skempton's *B* do not change.

The lowest pore pressure at a stage when the Skempton's *B* starts to level off can be taken as the pore pressure threshold when the pore fluid linearity is achieved. And this

pore pressure can be set as the initial pore pressure (or backpressure) for the Skempton's *B* measurement under different effective stress levels (see the next Section 3.1.4). Figure 5 presents some typical curves to explain this part's work.

However, if the test results show that there is significant air still trapped in the pore fluid system, one would need to repeat the steps in Sect. 3.1.2 and repeat the de-air procedure to further reduce the air concentration. Otherwise, one can move on to the next section to perform the measurement of Skempton's *B* with the focus on the rock matrix.

3.1.4 Skempton's *B* Measurement Under Similar Backpressure but Different Effective Stress

This step aims to measure the Skempton's *B* at different effective stress conditions and establish a correlation between the Skempton's *B* and effective stress. The initial pore pressure (back pressure as set by both the upstream and downstream pumps) was set at a fixed value determined as described in Sect. 3.1.3 for each run and the confining pressure was increased stepwise. In such test, the obtention of different Skempton's *B* is caused by the different effective stress only, with no impact from the pore fluid compressibility because the fluid compressibility remains stable at a similar back pressure level. Generally, the threshold of the back pressure (initial pore pressure) for a well de-aired sample could be around 150–200 psi (Mesri et al. 1976). We usually use 500 psi (or above) as the back pressure for this work to ensure no free air exists in the pore fluid system.
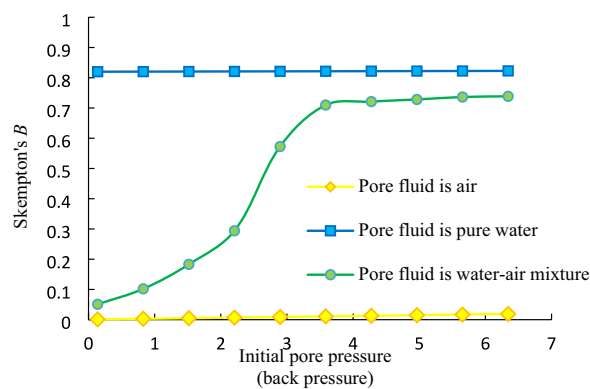
Fig. 5 Typical Skempton's B behaviors with different types of pore fluids: when the pore fluid is air, Skempton's B is extremely low, close to zero; when the pore fluid is pure water, Skempton's B remains at a relatively consistent high value; when the pore fluid is a mixture of water and air, it shows a curved line somewhere in between, and the shape and position of this line varies depending on the air concentration. When the air is totally dissolved into the water, the curve will asymptotically approach the pure water line

20) Set both the upstream pump and downstream pump pressures at 600 psi (4.14 MPa) as the back pressure, set the confining pressure at 800 psi (5.52 MPa) and the pore pressure can be taken as 600 psi (4.14 MPa) when a pressure equilibrium condition between the sample and the pumps is reached. Note the pore pressure 600 psi (4.14 MPa) as used in this test is sufficiently high to ensure the consistent compressibility of the pore fluid during the measurement without any free air in the system. After pore pressure stabilization, shut off the valves (V3 and V5) to isolate the rock/pressure transducer system from the upstream/downstream pumps.

21) Increase the confining pressure quickly to a higher value and record the pressure transducer's reading, correspondingly. The ratio between pore pressure and confining pressure change will yield a Skempton's *B* value that's related with this effective stress (the difference between confining pressure and back pressure).

22) The tests can be run at different starting points with similar back pressure (initial pore pressure) but different confining pressure (thus different effective stress). The difference of averaged confining pressure and pore pressure for a run can be taken as the effective stress in which the Skempton's *B* is related, and the stress dependency feature of the Skempton's *B* can be revealed after a series of tests with different starting points.

3.2 Biot's Effective Stress Coefficient Measurement

The schematic laboratory set-up is described in Fig. 6. The main parts include a MTS 315 integrated cell with a data acquisition system, three Teledyne ISO syringe pumps, a pore fluid storage tank and a set of strain gauge measurement components. They are connected by a few pipes, valves, and signal lines.

For this test, another dry sample (Sample C) was used. Since the rock's permeability is extremely low in the nano-Darcy range, argon is used as the pore fluid. As an inert gas, argon has the advantage to ensure pore pressure equilibrium in a relatively short time frame and also to avoid any physicochemical reactions between the rock matrix and the pore fluid, including gas absorption effect and fines migrations during fluid flow, etc. The pore pressure was kept at a minimum value of 800 psi/5.52 MPa, which is above argon's supercritical pressure (argon behaves more like a liquid above the critical point of 150 K/– 123 °C and 705 psi/4.86 MPa). Brace et al. (1968) showed that permeability tested by water on Westerly granite was similar to that by argon at high pore pressures when the argon is in its supercritical status.

1) Prepare a right cylindrical sample with a height-to-diameter ratio of 1.5–2.5 (in this case it is 1.8), which is in the favorable range for a conventional geo-mechanical testing (ISRM 2007; ASTM D4543-08 2008). The end face flatness (surface profile) is smooth to ± 0.01 mm and free

Fig.6 Test configuration for the Biot's effective stress coefficient measurement
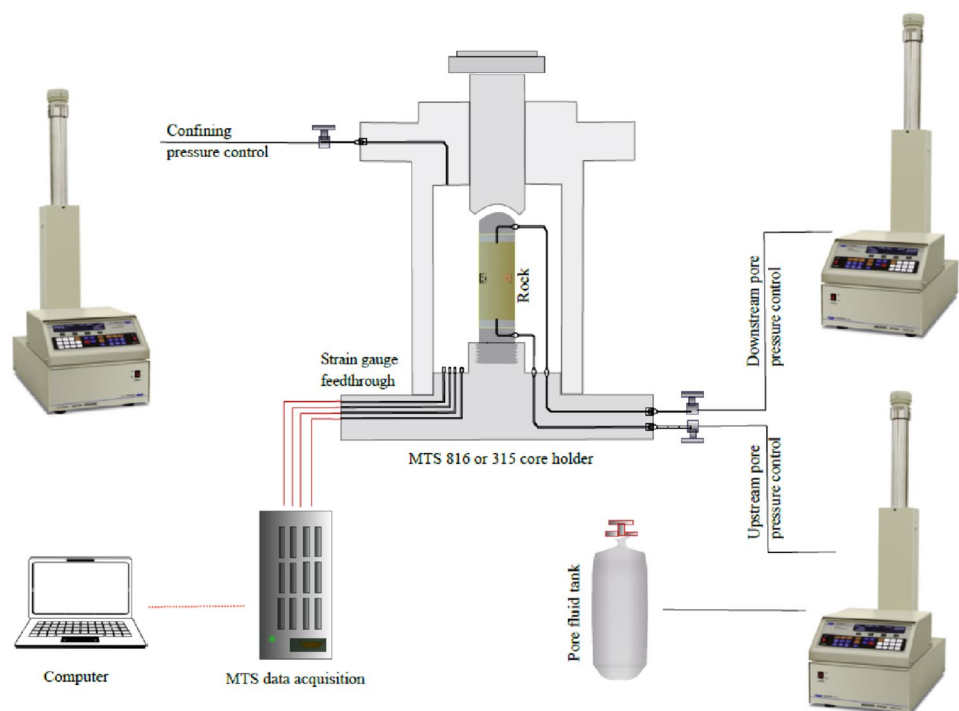
of any abrupt irregularities. The side of the specimen is also smooth and free of any abrupt irregularities.

2) Use two steel platens on both ends of the sample with circular porous sintered metal plate placed between the sample and the steel platen. Cover the lateral surface with ultrathin copper shim (0.003inch / 0.076 mm). Use epoxy to seal the whole set-up. After the epoxy consolidates, put the sample into the core holder and apply high confining pressure (1000 psi/6.89 MPa) to ensure the copper shim attached tightly on the sample surface. Ensure the sample is isolated from the confining fluid during this process.

3) After taking the sample out of the core holder, glue two sets of biaxial strain gauges on the lateral surface and ensure the axial direction of the gauge and the sample's vertical axis strictly in parallel. The volumetric strain is calculated by adding the averaged axial strain and two radial strains. In case some gauges yield non-linear and/ or extremely high or low values that is probably more a localized phenomenon, the experimenter may need to report both averaged results and the results by excluding those "abnormal" readings.

4) Put the sample in the core holder, connect the platens with the upstream/downstream pumps and the strain gauges with the feedthroughs. Check the signal quality and then close the cell.

5) For the purpose of the Biot's coefficient measurement, the grain bulk modulus, drained bulk modulus and the poroelastic expansion coefficient are needed. The grain bulk modulus is measured using a jacketed test with pore pressure always 100 psi lower than the confining pressure and recording the volumetric strain as measured by the strain gauges.

6) The drained bulk modulus K is a measure of the stiffness of the porous solid frame upon dry or constant pore pressure condition. While maintaining a constant pore pressure, the confining pressure is increased from a low level to high level and the strain is recorded during this process. The loading rate should be low enough to ensure a drained condition. The maximum effective stress should cover the in-situ effective stress level of the sample if the sample is from a deep depth.

7) Poroelastic expansion coefficient H is the ratio of pore pressure change over the volumetric strain under a constant confining pressure condition. H is the counterpart of K but is measured under constant confining pressure by varying the pore pressure. Maintaining a constant confining pressure at a high level, the pore pressure is set close to the confining pressure, and then decreases slowly to a low level. The volumetric strain is recorded during this process. The loading rate should be low enough to ensure the pore pressure decreases in a quasi-static manner. The poroelastic expansion coefficient H

can be evaluated from the slope of the effective stress vs volumetric strain curve. The confining and pore fluid pressure are recorded by the Agilent data acquisition system at a frequency of one data point per second.

4 Laboratory Test Result

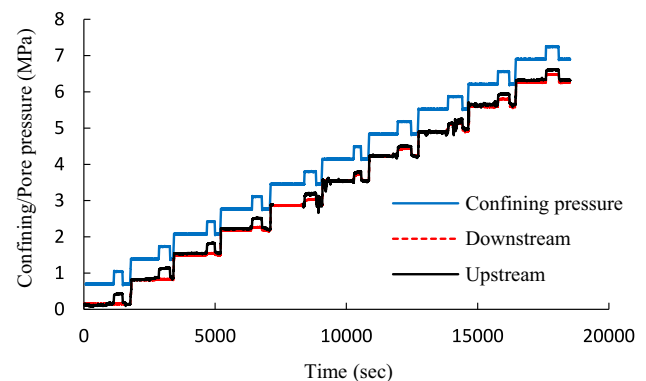### 4.1 Skempton's B Measurement Results

The test results of Skempton's B are grouped into the following two sections.

#### 4.1.1 Skempton's B Under Constant Effective Stress Condition

Following the laboratory test protocol described in Sect. 3.1.3, the test results are reported in Figs. 7 8, 9, 10 and Table 3.

For the first round of testing, one can see that the pore pressure responses in the upstream and downstream of the sample are different, with one side much more sensitive to the confining pressure increment than another side (Fig. 7; Table 3 (1st run)); such difference indicates water at one side is better de-aired than another side, and further de-air work is needed. The Skempton's B behavior that is based on this stage of testing is summarized in Fig. 8. Because of the very low permeability, the pore pressure responses on both sides of the sample are different, and independent with respect to each other under a quickly undrained condition.
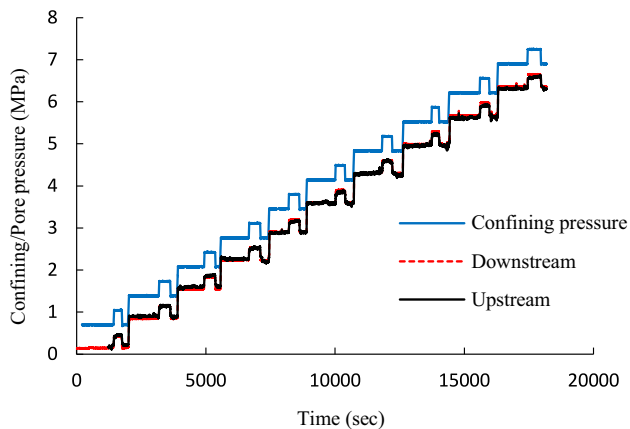
The test results (Table 3, 1st run and Figs. 7 and 8) clearly show that there is some air still trapped in the pore system after the sample installation and initial de-air process, especially in the downstream section. Thus, further de-air work

Fig.7 Skempton's B measurement after sample installation and initial de-aired work (In this loading path, the pore pressure responses to the confining pressure increase are different on the two sides of the sample, indicating one side (upstream) is better saturated with water than the other side (downstream); and further de-air work is needed on the downstream section to reduce the air concentration)
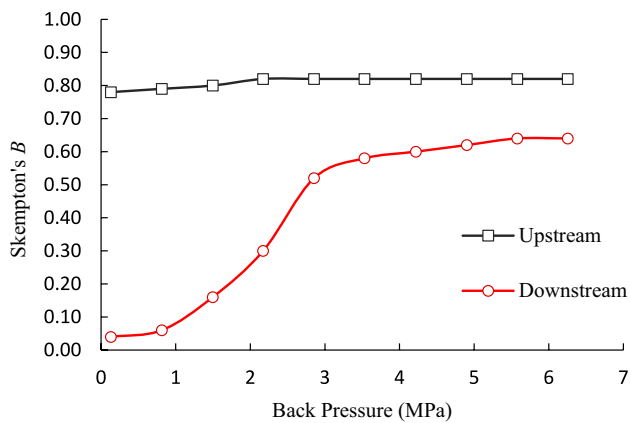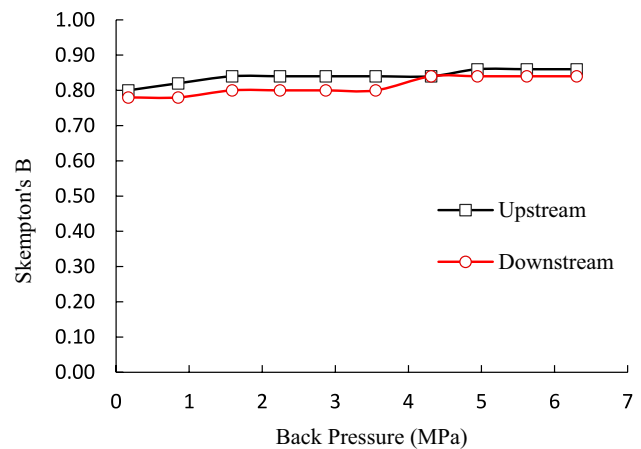
Fig.8 Skempton's B behavior based on Fig. 7 (In the upstream section, the pore fluid is pure water thus yielding a consistent Skempton's B value; while in the downstream section, Skempton's B increases with the back pressures, indicating a condition of the pore water trapped with some air)

Fig.10 Skempton's B behavior based on Fig. 9 (The change in downstream Skempton's B behavior is obvious to compare with Fig. 7, indicating a condition of the pore fluid trapped with some air (Fig. 8) and a condition with the pore fluid depleted from air (Fig. 10))

Fig. 9 Skempton's B test after further de-air procedure (fluid pressure responses to the confining pressure increase are the same on both sides of the sample, and very sensitive to the confining pressure change even at very low-pressure level, indicating the pore fluid system is well de-aired. An air-free water saturation has been achieved)

had to be conducted, including a lengthy core flooding process and using the vacuum pump to suck the air out of the system in the downstream section.

To verify if the pore water is air-free, another round of measurements following the similar procedure of the first round of test was performed, and the test result is shown in Fig. 9, 10 and Table 3 (2nd run). Compare Fig. 8 with Fig. 10, the difference is obvious. In Fig. 10, both sides of the sample respond to the confining pressure increase more promptly and similarly, and such responses are insensitive to the back pressure levels, indicating the fluid in the porous space is depleted with air; a linear fluid compressibility has been achieved even at a very low back pressure level.

When there is air trapped in the pore water system, Skempton's B increases significantly from low pore pressure level to high pore pressure level because of the pore fluid compressibility changing greatly with the fluid pressure when air exists in the pore system. However, once the air is depleted, the pore fluid compressibility tends to be constant, and insensitive to the pressure change. Skempton's B stabilized at 0.84 to 0.86 at high pressure levels for both sides. Note the effective stress for each round of test is all the same around 80 psi (0.55 MPa), which is very small. When there is air trapped in the pore fluid, the air concentration in the pore fluid system varies at different back pressure levels, thus the Skempton's B is not unique even the effective stress level was maintained the same (as shown in the first run in Table 3). However, once air is depleted from the system, the Skempton's B becomes much more consistent under such loading path with a consistent effective stress level (as shown in the second run in Table 3).

4.1.2 Skempton's *B* Under Constant Back Pressure Condition

Based on the test results (Fig. 10), the fluid compressibility has shown a linear trend even at a very low pore pressure level after a lengthy de-aired work (less than 100 psi/0.69 MPa; Fig. 10). However, to ensure good test results, a back pressure of 600 psi (4.14 MPa) is taken as a threshold, above which full saturation of the sample with water is completely achieved (Note in Fig. 10, there are still small increases of Skempton's B above 4 MPa). Thus, in this part's tests for Skempton's B, the initial pore pressure for each test was set to 600 psi (4.14 MPa). The test procedure is detailed in Sect. 3.1.4. The test results
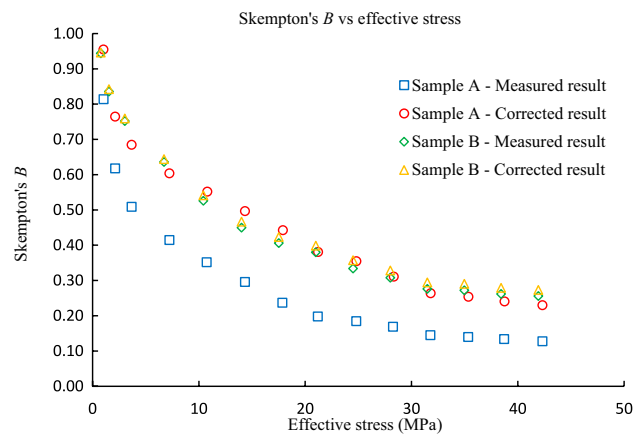
Table 3 Skempton's *B* measurement of Sierra White granite (Sample A) at different back pressure with similar effective stress levels

	Effective stress		Back pressure	Confining pressure Pc (psi)		Upstream fluid pressure Pp (psi)		Upstream Skempton's B	Downstream fluid pressure Pp (psi)		Downstream Skempton's B
Test #	Psi	MPa	MPa	Start	End	Start	End		Start	End	
Correlation between Skempton's B and back pressure—First run											
Test 1	79	0.54	0.15	100	150	24	63	0.780	19	21	0.040
Test 2	78	0.53	0.84	200	250	127	167	0.790	118	121	0.060
Test 3	79	0.54	1.52	300	350	225	265	0.800	217	225	0.160
Test 4	81	0.56	2.20	400	450	324	365	0.820	315	330	0.300
Test 5	81	0.56	2.89	500	550	425	466	0.820	414	440	0.520
Test 6	84	0.58	3.56	600	650	521	562	0.820	512	541	0.580
Test 7	87	0.60	4.23	700	750	615	656	0.820	612	642	0.600
Test 8	86	0.59	4.93	800	850	718	759	0.820	711	742	0.620
Test 9	88	0.61	5.60	900	950	815	856	0.820	809	841	0.640
Test 10	90	0.62	6.27	1000	1050	913	954	0.820	907	939	0.640
Correlation between Skempton's B and back pressure—Second run											
Test 1	77	0.53	0.16	100	150	22	62	0.800	24	63	0.780
Test 2	77	0.53	0.85	200	250	123	164	0.820	123	162	0.780
Test 3	74	0.51	1.56	300	350	223	265	0.840	230	270	0.800
Test 4	76	0.52	2.23	400	450	323	365	0.840	325	365	0.800
Test 5	81	0.56	2.89	500	550	422	464	0.840	416	456	0.800
Test 6	81	0.56	3.58	600	650	523	565	0.840	515	555	0.800
Test 7	76	0.52	4.31	700	750	624	666	0.840	625	667	0.840
Test 8	80	0.55	4.96	800	850	723	766	0.860	717	759	0.840
Test 9	81	0.56	5.65	900	950	823	866	0.860	815	857	0.840
Test 10	83	0.57	6.33	1000	1050	921	964	0.860	914	956	0.840

* Note Figures 7, 8 are the visualization of the 1st run, and Figure 9, 10 are for the 2nd run, respectively. In all these tests, the effective stresses (= confining pressure—pore pressure) were very small, around 80 psi (0.55 MPa). The back pressure refers to the initial pore pressure at each stage

are summarized in Fig. 11 and Table 4. Undrained pore pressure increases due to hydrostatic compression involve both poroelastic and poroviscoelastic effects with the viscous effects more pronounced at high effective stress levels (Makhnenko and Podladchikov 2018). Thus, the readings of the fluid pressures were picked at 20 s after the confining pressure reached its target value at each stage to mainly reflect the poroelastic effect.

For crystalline rock, the pores are dominated by microcracks with high aspect ratio with a small portion of pores which are much stiffer. Thus, the porosity of rock decreases sharply with increasing effective stress at the beginning but approaches an asymptotic value when those compliant cracks are sealed, leaving the robust openings to sustain the pressure. The behavior of Skempton's *B* reflects such a characteristic of the porous structure of this type of rock.

Fig.11 Skempton's B of Sierra White granite as a function of effective stress. Sample A was tested in a system with a dead volume of 4.75 ml, and Sample B was tested in a system with a dead volume of 0.80 ml. Sample A's result after correction is very close to that of Sample B's. The correction for Sample A is obvious but for Sample B is very subtle and much smaller

Table 4 Skempton's B measurement of Sierra White granite (Sample A) at different effective stress under water saturation

Test #	Confining pressure (psi)	Upstream measurement				Downstream measurement			
		Pore pressure (psi)	Effective stress		Skempton's B	Pore pressure (psi)	Effective stress		Skempton's B
			psi	MPa			psi	MPa	
1	800	590				590			
	1300	898	306	2.11	0.616	900	305	2.10	0.620
2	1000	592				593			
	1500	847	531	3.66	0.510	847	530	3.65	0.508
3	1500	601				597			
	2000	805	1047	7.22	0.408	808	1048	7.22	0.422
4	2000	604				592			
	2500	784	1556	10.73	0.360	764	1572	10.84	0.344
5	2500	600				596			
	3000	745	2078	14.33	0.290	747	2079	14.33	0.302
6	3000	601				591			
	3500	725	2587	17.84	0.248	704	2602	17.94	0.226
7	3500	626				623			
	4000	730	3072	21.18	0.208	717	3080	21.24	0.188
8	4000	603				606			
	4500	703	3595	24.79	0.200	691	3601	24.83	0.170
9	4500	609				592			
	5000	698	4097	28.25	0.178	672	4118	28.39	0.160
10	5000	607				601			
	5500	678	4608	31.77	0.142	675	4612	31.80	0.148
11	5500	590				589			
	6000	664	5123	35.32	0.148	655	5131	35.37	0.132
12	6000	600				598			
	6500	670	5614	38.71	0.140	662	5624	38.77	0.128
13	6500	586				590			
	7000	656	6136	42.31	0.138	648	6135	42.30	0.116
14	800	695				703			
	1300	1107	149	1.03	0.824	1105	146	1.01	0.804

4.1.3 Correction of the Skempton's B Test Result

Due to the existence of the dead volume (platens, pipes, transducers, and connection fittings, etc.), one may take the measurement to represent the lower limit of the "true" Skempton's B requiring data correction as described in this section. The correction is based on the following Eq. 7 from Ghabezloo and Sulem (2010). This equation is close to the equation of Bishop (1976) with an addition of the term "κ_L" which also takes the influence of the confining pressure on the dead volume into account.

$$B^{cor} = \frac{B^{mes}}{1 + \frac{V_L \rho_{fL}}{V \rho_f (c_d - c_s)} \left[\kappa_L - B^{mes}(c_{fL} + c_L) \right]} \quad (7)$$

where V is the rock bulk volume, V_L is the dead volume, ρ_f is the pore fluid density, ρ_{fL} is the fluid density in the drainage system. c_d, c_s are the elastic compressibility coefficient of rock, with $c_d = \frac{1}{K}$, $c_s = \frac{1}{K_s'}$. c_L and κ_L are the isothermal compressibility of the drainage system defined by the following equations, $c_L = \frac{1}{V_L}\left(\frac{\partial V_L}{\partial P_f}\right)_{T,\sigma}$ and $\kappa_L = -\frac{1}{V_L}\left(\frac{\partial V_L}{\partial \sigma}\right)_{T,p_f}$ respectively. c_L and κ_L are conceptually in parallel with $1/H$ and $1/K$ for the rock, which can be written as: $c_L = \frac{1}{H_L}$; $\kappa_L = \frac{1}{K_L}$ with the subscript "L" standing for the drainage system. c_{fL} is the fluid compressibility in the drainage system. This equation can be simplified if the fluid densities in the drainage system and rock pores are the same ($\rho_{fL} = \rho_L$), and replace the compressibility with their corresponded moduli ($c_d - c_s = \frac{1}{K} - \frac{1}{K_s'} = \frac{1}{H}$; H is poroelastic expansion coefficient (Wang 2000); $c_{fL} = c_f = \frac{1}{K_f}$ where K_f is the fluid bulk modulus):

$$B^{cor} = \frac{B^{mes}}{1 - \frac{HV_L}{V}\left[B^{mes}(\frac{1}{K_f} + \frac{1}{H_L}) - \frac{1}{K_L}\right]} \quad (8)$$

Here, H, B^{mes}, V_L, V, K_f, H_L, K_L are all needed in order to get the corrected B (B^{cor}). Since many terms in this equation are stress dependent, only the terms tested at similar effective stress level are to be used for corrections to be meaningful. Laboratory tests on the drainage system without the sample have been performed to obtain V_L, H_L and K_L. B^{mes} is taken as the average of the upstream and downstream readings as these two sets of readings are very close, while the correction tests treat the drainage system as a single system without the separation of upstream and downstream sections. The drainage system is complicated not only because it includes many different parts (platens, pipes, transducers and connection fittings). Also, a part of it is in the cell (can be influenced by the confining pressure) and part of it is out of the cell (without any impact from the confining pressure).

It was found that similarly to the rock's drained bulk modulus, K_L shows a stress stiffening behavior, with relatively small values at the low effective stress levels which increases in an exponential manner with effective stress. In regard to the correction Eq. (8), K_L has a large role at the low effective stress levels but it tends to diminish when the effective stress increases. H_L is relatively insensitive to the effective stress, and falls within a relatively narrow range, indicating the internal fluid pressure and volume changes are not sensitive to the effective stress changes (or the increase of the cell pressure, P_c). Since the drainage system involves the sections of different materials and shapes, especially the connection fittings, which are all difficult to quantify from

a mathematical approach, an actual test is needed to reveal their combined behavior and resolve these input parameters.

The sample bulk volume is $V = 81.93 \text{cm}^3$ based on the sample dimension and in fact, V is also stress dependent, but its change with effective stress is so small (less than 0.16% based on the measured volumetric strain) that it can be treated as a constant for this correction. The dead volume V_L is measured as 4.75 ml and the fluid bulk modulus K_f is 2.00GPa. H is estimated based on the test results of the same type of rock (Sample C) retrieved from the same block of this sample. Then, the following Table 5 for the purpose of correction is established.

The corrected result and the tested results can be compared in the following Fig. 11. Based on the input parameter sensitivity analysis, it was found that the laboratory test accuracy is firstly influenced by the dead volume V_L. When this value is relatively small, the error can be greatly reduced. Therefore, another Sierra sample retrieved from the same block (Sample B, length 72.6 mm, diameter of 37.70 mm) was tested following the same procedure using a newly manufactured steel cell with a much smaller dead volume of 0.80 ml. The results from the test in this cell (using averaged upstream and downstream readings) and the corrected result from the previous tests are plotted in this figure for comparison.

4.2 Biot's Effective Stress Coefficient

This part presents the results of the measurements of the grain bulk modulus, K'_s, drained bulk modulus, K, and the poroelastic expansion coefficient, H, from which the Biot's effective stress coefficient, α, can be derived.

Table 5 Summary of the correction results

Effective stress	B^{mes}	H	K_L	H_L	K_f	Final correction coefficient	B^{cor}
MPa		GPa	GPa	GPa	GPa		
2.11	0.618	10.40	2.41	1.48	2.00	1.231	0.761
3.66	0.509	14.35	3.38	1.49	2.00	1.333	0.678
7.22	0.415	22.74	4.02	1.52	2.00	1.440	0.598
10.79	0.352	26.66	5.74	1.54	2.00	1.553	0.547
14.33	0.296	34.65	7.18	1.57	2.00	1.656	0.490
17.89	0.237	41.50	12.99	1.60	2.00	1.839	0.436
21.21	0.198	46.45	21.89	1.62	2.00	1.897	0.376
24.81	0.185	50.19	23.36	1.65	2.00	1.890	0.350
28.32	0.165	52.86	33.20	1.67	2.00	1.863	0.307
31.79	0.145	53.88	60.96	1.70	2.00	1.791	0.260
35.35	0.140	54.68	87.07	1.72	2.00	1.797	0.252
38.74	0.135	55.35	104.21	1.75	2.00	1.765	0.238
42.31	0.128	56.66	134.61	1.77	2.00	1.780	0.228
1.02	0.814	7.54	1.58	1.47	2.00	1.167	0.950

4.2.1 Grain Bulk Modulus, K_s'

The measurement was done starting at a confining pressure of 900 psi (6.21 MPa) and reaching to 5000 psi (34.47 MPa) and then decreasing to 1500 psi (10.34 MPa). This was done in a stepwise manner using a pressure change of 100 psi (0.69 MPa) at each step. The pore pressure was maintained at 100 psi lower than the confining pressure all the time. This stress path took a total of 6 days because of the low permeability of the sample. The waiting time for every increment must be long enough to allow pore pressure equilibrium in the sample. A way for detecting minimum waiting time is to observe the strain gauge readings, until these readings remain stable without any further change over the elapsed time.

For a rock sample with very low permeability, pore fluid equilibrium may not be able to be achieved during the loading path but is likely realized during the unloading path based on the past experience. A very long linear section appeared along the unloading path with a consistent slope (Fig. 12), yielding a grain bulk modulus of 50.38 GPa, which is a reasonable result for the Sierra White granite by considering its mineral composition (Table 2).

Sierra White granite was mainly made of two types of minerals, one is quartz (about 44%), and another is albite (about 46%) (Table 2). Quartz's bulk modulus is relatively low, about 37–40 GPa (Hart and Wang 1995; Wang 2000), while albite's bulk modulus is much higher, about 70 GPa but can also vary depending on a more detailed mineral phase (Ahrens 1995; Pabst et al. 2015). Thus, the grain bulk modulus as measured in this work, 50 GPa, is a reasonable estimation for this type of rock.
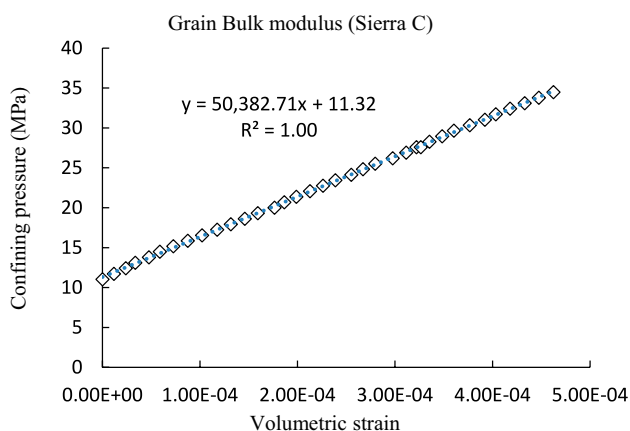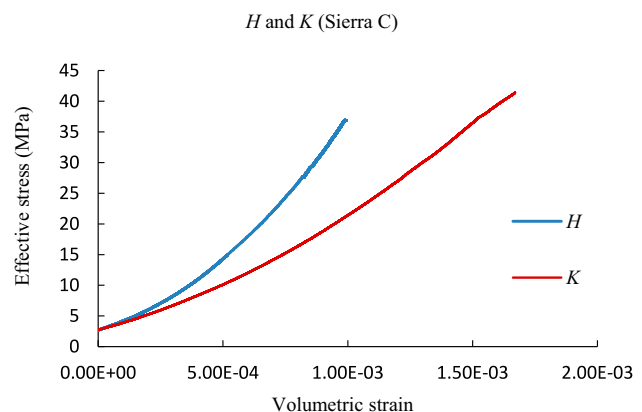
4.2.2 Drained Bulk Modulus, K

During the hydrostatic compression test, the loading curve usually shows a non-linear behavior, and consequently, bulk modulus can be separated into secant bulk modulus and tangent bulk modulus. Tangent parameter is used in view of the non-linear response of rocks, since non-linear tangent bulk modulus is highly stress dependent in comparison with secant bulk modulus. The tangent bulk modulus is approximated in a stepwise manner by calculating the slope of every small section along the loading path, and then the relationship between K and the corresponded effective stress can be established. Such nonlinearity of the drained bulk modulus is related to the evolution of microcrack compliance, which is rapid under relatively lower effective stress (usually less of 10 MPa), but as the micro-cracks evolve into less compliant features (i.e., equant features), the bulk response becomes less sensitive to the effective stress, and the stress–strain curve becomes straighter (Bernabe 1985; Zimmerman 1986).

Based on the Eq. (4), the Biot's effective stress coefficient can be calculated, and its relationship with the effective stress can also be established. The test was performed under 800 psi (5.52 MPa) pore pressure (constant) with confining pressure increased from 1200 psi (8.27 MPa) to 6800 psi (46.89 MPa) within 25 h at a loading rate of 3.8 psi/min. This loading rate is slow enough to maintain a drained condition. Figure 13 shows the drained bulk modulus test results; the curve is formed by 18,000 points with a data acquisition frequency of one point per five seconds.

4.2.3 Poroelastic Expansion Coefficient, H

The test was performed under 6400 psi (44.13 MPa) confining pressure with pore pressure decreasing from 6000 psi

Fig.12 Grain bulk modulus measurement of Sierra White granite (50.38 GPa)

Fig.13 Correlations of the effective stresses and the volumetric strains for drained bulk modulus K and poroelastic expansion coefficient H of Sierra White granite (Sample C)
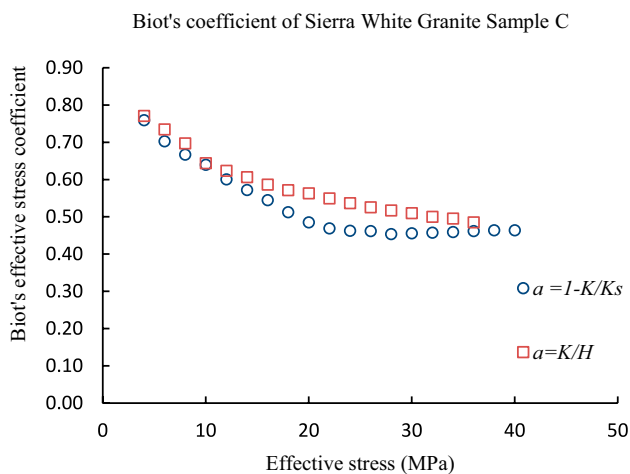
Fig.14 Biot's effective stress coefficient by two different approaches

Table 6 Test result summary for the Biot's effective stress coefficient

Effective stress	K	K'_s	α	H	A
MPa	GPa	GPa	$1 - K/K'_s$	GPa	K/H
4	12.12	50.38	0.76	15.72	0.77
6	14.98		0.70	20.39	0.73
8	16.78		0.67	24.07	0.70
10	18.14		0.64	28.16	0.64
12	20.12		0.60	32.27	0.62
14	21.55		0.57	35.52	0.61
16	22.92		0.55	39.08	0.59
18	24.57		0.51	42.97	0.57
20	25.93		0.49	46.03	0.56
22	26.75		0.47	48.69	0.55
24	27.08		0.46	50.43	0.54
26	27.12		0.44	51.57	0.53
28	27.51		0.46	53.17	0.52
30	27.41		0.46	53.74	0.51
32	27.33		0.46	54.66	0.50
34	27.24		0.46	54.96	0.50
36	27.11		0.46	55.88	0.49
38	27.01		0.46		
40	27.00		0.46		

(41.37 MPa) to 1000 psi (6.89 MPa) within 27 h at a constant loading rate of 3.3 psi/min. If the pore pressure path is transferred into effective stress path (effective stress = confining pressure—pore pressure), the following Fig. 13 can be achieved. Figure 13 can make K and H to be tied by the similar effective stress.

The two types of curves of K and H show similar features, i.e., all the curves show an increased slope over the increase of stress, and H curve generally has a higher slope than that of K curve. The Biot's coefficient can be evaluated by comparing K and H at the similar effective stress using Eq. (5).

4.2.4 Biot's Effective Stress Coefficient, *α*

The Biot's coefficient can be calculated based on the Eq. (4) and (5), its values as a function of the effective stress are displayed in Fig. 14 and Table 6.

Overall, the Biot's coefficient of the Sierra White granite sample decreases from 0.77 at low effective stress to 0.45–0.55 at high effective levels. The results from these two different approaches are not identical but close enough to establish confidence; note the differences vary within a range from 0 to 15%. Since rocks are not perfect homogeneous elastic materials, there probably always exist some sort of variations among the different loading–unloading paths due to the inhomogeneity and inelasticity, which may lead to the minor difference for the Biot's coefficients as measured by different approaches.

5 Discussion and Conclusion

In this work, a methodology has been developed and applied to measure the poroelastic properties including Skempton's B and the Biot's effective stress coefficient, α, of an ultra-low permeability rock, namely, the Sierra White granite. Unlike the Biot's coefficient, which is only a solid phase property, Skempton's B is a property related to both the properties of solid rock material and the pore fluid. Thus, there are two types of Skempton's B behavior from the laboratory testing standpoint: one is related with the pore fluid compressibility (and can be tested under different backpressure with a constant low effective stress) and another related to the rock matrix (and can be tested under constant backpressure with different effective stresses). One may not be able to simply compare these two types of measurements as they reflect different mechanisms. For example, a low Skempton's B such as 0.3 found in the red curve (Fig. 8) is caused by a low fluid compressibility, while a low Skempton's B of 0.3 in Fig. 11 is caused by the low porosity and very stiff rock structure at higher effective stress. In fact, as has been suggested (Green and Wang 1986), decreasing of the Skempton's B with increasing effective stress is related to the crack closure and/or high-compressibility materials within the rock framework.

At different back pressure but similar effective stress, the correlation between Skempton's B and pore pressure can reveal the impact of the pore fluid to Skempton's B. Increasing pore pressure will increase the pore fluid compressibility, thus Skempton's B will increase with the increase of pore pressure. However, if the pore fluid is depleted with air, the fluid compressibility will not be sensitive to the fluid

pressure change, and a leveled line will be present. Using this technique, one can determine if air is trapped in the pore fluid system and assess its severity. De-airing process should be implemented to reduce the air concentration in the pore fluid system to make the fluid as pure as possible, because Skempton's B is nonunique when the pore fluid compressibility varies. For a similar back pressure at different confining pressures, the correlation between Skempton's B and effective stress reveals the impact of rock matrix on Skempton's B. Increasing the effective stress reduces the porosity, thus decreasing the Skempton's B.

The procedure described is a relatively complete testing protocol for the Skempton's B measurement, with the consideration of both pore fluid and rock matrix. The combination of these two types of Skempton's B measurements can give a more in-depth and complete understanding of the Skempton's B behavior for a rock sample. In fact, considering Eq. (2), one can see that for the first type of measurement, the boundary condition is the constant effective stress which can guarantee the rock frame properties remain constant (K, K_s', K_s'' and ϕ), thus the variation of B is caused by the change of K_f at different back pressures. While in the second type of measurement, the boundary condition is the constant back pressure that provides a constant K_f, then the change of K and ϕ at different effective stress can yield different values of B. Note K_s' and K_s'' are generally insensitive to the stress change and can be taken as the constants from the laboratory testing standpoint. The methodology as described in this paper is applicable to any rock type except some water sensitive ones, either with chemically reactive minerals or swelling clays, or both. The accuracy of the measurement is mainly influenced by the dead volume of the drainage system. Reducing the dead volume can greatly reduce the error of the measurement. The impact of the stiffness (or the compressibility) of the drainage system to the measurement is complicated and special tests are needed to obtain their behavior for the purpose of correction. If the dead volume is very small, a correction may not be very necessary from a laboratory testing standpoint.

For the Sierra White granite sample tested, the Biot's coefficient measurement, grain bulk modulus K_s' shows a linear behavior, while both drained bulk modulus K and poroelastic expansion coefficient H show non-linear behaviors and are stress dependent. The measured grain bulk modulus of 50 GPa is appropriate for this sample by considering its mineralogical compositions that are dominated by quartz and albite. Similarly to that of Skempton's B, the Biot's effective stress coefficient also shows a stress dependent feature. The Biot's effective stress coefficient varies in a range of 0.77 down to 0.45–0.55 with the increase of the effective stress.

Declarations

References

Adachi K (1974). Influence of pore water pressure on the engineering properties of intact rock. PhD Dissertation, University of Illinois at Urbana-Champaign.

Ahrens TJ (1995) Mineral Physics and Crystallography: a handbook of physical constants. American Geophysical Union, Washington, DC

ASTM (2004) Standard test method for consolidated undrained triaxial compression test for cohesive soils. ASTM D4767. ASTM, West Conshohocken, PA

ASTM D4543-08 (2008) Standard practices for preparing rock core as cylindrical test specimens and verifying conformance to dimensional and shape tolerances. American Society for Testing and Materials, West Conshohocken, PA

Battino R, Rettich TR, Tominaga T (1984) The solubility of nitrogen and air in liquids. J Phys Chem Ref Data 13(2):563–600. https://doi.org/10.1063/1.555713

Berge PA, Wang HF, Bonner BP (1993) Pore pressure buildup coefficient in synthetic and natural sandstones. Int J Rock Mech Mining Sci Geomech Abstr 30:1135–1141. https://www.sciencedirect.com/science/article/abs/pii/014890629390083P

Bernabe Y (1985) Permeability and pore structure of rock under pressure. PhD Thesis, Massachusetts Institute of Technology. https://dspace.mit.edu/bitstream/handle/1721.1/57818/14925614-MIT.pdf?sequence=2

Berryman JG, Milton GW (1991) Exact results for generalized Gassmann's equations in composite porous media with two constituents. Geophysics 56:1950–1960. https://library.seg.org/doi/https://doi.org/10.1190/1.1443006

Biot MA, Willis DG (1957) The elastic coefficients of the theory of consolidation. J Appl Mech ASME 24:594–601. https://doi.org/10.1115/1.4011606

Biot MA (1941) General theory of three-dimensional consolidation. J Appl Phys 12(2):155–164. https://aip.scitation.org/doi/https://doi.org/10.1063/1.1712886

Bishop AW (1973) The influence of an undrained change in stress on the pore-pressure in porous media of low compressibility. Geotechnique 23(3):435–442. https://doi.org/10.1680/geot.1973.23.3.435

Bishop AW (1976) Influence of system compressibility on observed pore pressure response to an undrained change in stress in saturated rock. Geotechnique 26(2):371–375. https://doi.org/10.1680/geot.1976.26.2.371

Blöcher G, Bruhn D, Zimmerman G, McDermott C, Huenges E (2007) Investigation of the undrained poroelastic response of sandstones to confining pressure via laboratory experiment, numerical simulation and analytical calculation. Geol Soc 284:71–87 (**In Rock Physics and Geomechanics in the Study of Reservoirs and Repositories, eds. C. David and M. Le Ravalec-Dupin**)

Blöcher G, Reinsch T, Hassanzadegan A, Milsch H, Zimmermann G (2014) Direct and indirect laboratory measurements of poroelastic properties of two consolidated sandstones. Int J Rock Mech Min Sci. 67:191–201. https://www.sciencedirect.com/science/article/abs/pii/S1365160913001482

Brace WF, Walsh JB, Frangos WT (1968) Permeability of granite under high pressure. J Geophys Res 73:2225–2236. https://doi.org/10.1029/JB073i006p02225

Brace WF, Silver E, Hadley K, Goetze C (1972) Cracks and pores: a closer look. Science 178(4057): 162–164. https://www.science.org/doi/https://doi.org/10.1126/science.178.4057.162

Brown RJS, Korringa J (1975) On the dependence of the elastic properties of a porous rock on the compressibility of the pore fluid. Geophysics 40:608–616. https://doi.org/10.1190/1.1440551

Cheng AHD (1997) Material coefficients of anisotropic poroelasticity. Int J Rock Mech Min Sci 34(2):199–205. https://www.sciencedirect.com/science/article/abs/pii/S0148906296000551

Cheng AHD (2016) Poroelasticity, Theory and Applications of Transport in Porous Media. Springer International Publishing Switzerland.

Cheng AHD, Abousleiman Y, Roegiers JC (1993) Review of some poroelastic effects in rock mechanics. Int J Rock Mech Mining Sci 30 (7):1119–1126. https://www.sciencedirect.com/science/article/abs/pii/014890629390081N

Coussy O (2004) Poromechanics. John Wiley & Sons Ltd.

Feng X, Haimson B, Li X, Chang C, Ma X, Zhang X, Ingraham M, Suzuki K (2019) ISRM suggested method: determining deformation and failure characteristics of rocks subjected to true triaxial compression. Rock Mech Rock Eng 52:2011–2020. https://doi.org/10.1007/s00603-019-01782-z

Ghabezloo S, Sulem J (2010) Effect of the volume of the drainage system on the measurement of undrained thermo-poro-elastic parameters. Int J Rock Mech Min Sci 47:60–68

Ghassemi A, Tao Q, Diek A (2009) Influence of coupled chemo-poro-thermoelastic processes on pore pressure and stress distributions around a wellbore in swelling shale. J Pet Sci Eng 67(1–2):57–64. https://doi.org/10.1016/j.petrol.2009.02.015

Green HG, Wang HF (1986) Fluid pressure response to undrained compression in saturated sedimentary rock. Geophysics 51(4):948–956. https://doi.org/10.1190/1.1442152

Hart DJ, Wang HF (1995) Laboratory measurements of a complete set of poroelastic moduli for Berea sandstone and Indiana limestone. J Geophys Res Solid Earth 100(B9):17741–17751. https://doi.org/10.1029/95JB01242

Hart DJ, Wang HF (2001) A single test method for determination of poroelastic constants and flow parameters in rocks with low hydraulic conductivities. Int J Rock Mech Min Sci 38(4):577–583. https://doi.org/10.1016/S1365-1609(01)00023-5

Hart DJ, Wang HF (2010) Variation of unjacketed pore compressibility using Gassmann's equation and an overdetermined set of volumetric poroelastic measurements. Geophysics 75:9–18. https://doi.org/10.1190/1.3277664

Hu L, Ghassemi A (2020) Heat production from lab-scale enhanced geothermal systems in granite and gabbro. Int J Rock Mech. https://doi.org/10.1016/j.ijrmms.2019.104205. (**ISSN 1365-1609**)

ISO 286-1-2010 (2010) Geometrical product specifications (GPS)—ISO code system for tolerances on linear sizes—part 1: basis of tolerances, deviations and fits.

ISRM (2007) The complete ISRM suggested methods for rock characterization, testing and monitoring. In: Ulusay R, Hudson JA (eds) Suggested methods. Prepared by ISRM commission on testing methods. Compilation Arranged by ISRM Turkish National Group, Ankara

Jaeger JC, Cook NGW, Zimmerman RW (2007) Fundamentals of rock mechanics, 4th edn. Blackwell Publishing Ltd., Malden USA

Makhnenko RY, Podladchikov Y (2018) Experimental poroviscoelasticity of common sedimentary rocks. J Geophys Res Solid Earth 123(9):7586–7603. https://doi.org/10.1029/2018jb015685

Makhnenko RY, Tarokh A, Podladchikov Y (2017) On the unjacketed moduli of sedimentary rock. In: Vandamme M, Dangla P, Pereira JM, Ghabezloo S (eds) Poromechanics VI—Proceedings of the 6th Biot Conference on Poromechanics. American Society of Civil Engineers, Reston VA, pp 897–904

Mavko G, Mukerji T, Dvorkin J (2009) The rock physics handbook: tools for seismic analysis of porous media. Cambridge University Press, Cambridge, p I–IV

Mesri G, Adachi K, Ullrich CR (1976) Pore-pressure response in rock to undrained change in all-round stress. Geotechnique 26(2):317–330. https://doi.org/10.1680/geot.1976.26.2.317

Pabst W, Gregorova E, Rambaldi E, Bignozzi MC (2015) Effective elastic constants of plagioclase feldspar aggregates in dependence of the Anorthite content—a concise review. Ceramics—Silikáty 59(4):326–330. https://www.ceramics-silikaty.cz/2015/pdf/2015_04_326.pdf

Rice JR, Cleary MP (1976) Some basic stress-diffusion solutions for fluid-saturated elastic porous media with compressible constituents. Rev Geophys Space Phys 14:227–241. https://doi.org/10.1029/RG014i002p00227

Skempton AW (1954) The pore pressure coefficients A and B. Geotechnique 4:43–147. https://doi.org/10.1680/geot.1954.4.4.143

Tarokh A, Detournay E, Labuz J (2018) Direct measurement of the unjacketed pore modulus of porous solids. Proc R Soc A 474(2219):20180602. https://doi.org/10.1098/rspa.2018.0602

Wang HF (2000) Theory of linear poroelasticity with applications to geomechanics and hydrogeology. Princeton University Press

Ye Z, Ghassemi A (2018) Injection-induced shear slip and permeability enhancement in granite fractures. J Geophys Res. https://doi.org/10.1029/2018JB016045

Zhou X, Ghassemi A (2022) Experimental Determination of Poroelastic Properties of Utah FORGE Rocks. 56th US Rock Mechanics/Geomechanics Symposium held in Santa Fe, New Mexico, USA, 26–28, p 12

Zhou X, Vachaparampil A, Ghassemi A (2015) A Combined Method to Measure Biot's Coefficient for Rock. 49th US Rock Mechanics/Geomechanics Symposium held in San Francisco, CA, USA, 23–26. https://onepetro.org/ARMAUSRMS/proceedings-abstract/ARMA15/All-ARMA15/ARMA-2015-584/65861

Zhou X, Ghassemi A, Riley S, Roberts J (2017) Biot's Effective Stress Coefficient of Mudstone Source Rocks. 51st US Rock Mechanics/Geomechanics Symposium held in San Francisco, California, USA, 25–28, p 11. https://onepetro.org/ARMAUSRMS/proceedings-abstract/ARMA17/All-ARMA17/ARMA-2017-0235/124216

Zimmerman RW (1986) Compressibility of two-dimensional cavities of various shapes. J Appl Mech 53(3):500–504. https://doi.org/10.1115/1.3171802